Vapor Phase Growth and Assembly of Metallic, Intermetallic, Carbon, and Silicon Nanoparticle Filaments

M. Samy El-Shall,* Victor Abdelsayed, Yezdi B. Pithawalla, and Edreese Alsharaeh

Department of Chemistry, Virginia Commonwealth University, Richmond, Virginia 23284-2006

Seetharama C. Deevi

Research Center, Chrysalis Technologies, Incorporated, Richmond, Virginia 23234

Received: October 2, 2002; In Final Form: January 13, 2003

A new class of nanoparticle filaments and tree-like aggregates is assembled by the influence of an electric field during the synthesis of metallic, intermetallic, silicon, and carbon nanoparticles from the vapor phase. Enormous electrostatic aggregation due to dipole forces is observed between the nanoparticles to form chain filaments, and between the chain filaments to form tree-like fibers. The filaments and tree-like fibers can grow to lengths exceeding several centimeters. The filaments display stretch and contraction properties depending on the strength of the applied field.

Nanoparticles often exhibit novel properties, which are different from the properties of the bulk material. Many of these properties show strong dependence on size, shape, and surface composition.[1−3] The assembly of nanoparticles into filaments and fibers that retain the unique properties of the nanoparticles holds promise for the development of novel functional materials and for the engineering of a variety of nanodevices and sensors.[4−6]

Several techniques utilizing electrodeposition, template growth in membrane channels, and capillary forces have been employed for the assembly of nanoparticles into wires and patterned structures, with the ultimate goal of fabrication of nanodevices such as sensors and circuits.[5−12] The assembly of colloidal nanoparticles by dielectrophoresis from suspensions has been recently reported.[10] Most of the published work has focused on gold nanoparticles and nanorods and carbon nanotubes.[10−12,13−17] While considerable effort has been devoted to colloidal nanoparticles suspended in liquid media, little work has addressed the assembly of nanoparticles from the vapor phase. Ferromagnetic iron and cobalt nanoparticle wires have been fabricated by thermally decomposing metal carbonyl vapors in the presence of a magnetic field.[18] Here, we describe a new approach that utilizes electric fields to assemble a wide variety of nanoparticles into wires, filaments, and fibers in the vapor phase. Specifically, we report the observation of long chain filaments and tree-like fibers of several metallic, intermetallic, silicon, and carbon nanoparticles under the influence of an electric field. The chains display stretch and contraction properties depending on the strength of the applied field. Introducing a reactive olefin monomer vapor during the synthesis and assembly of the nanoparticles leads to the formation of composite metallic/polymer filaments. The filament-like and tree-like assemblies may have some special applications as fillers (additives) to increase the elastic modulus and tensile strength of low-strength oils and polymeric materials. This may allow for stronger interactions between the polymer chains and the nanoparticle chain aggregates.

The nanoparticle filaments are grown using the laser vaporization controlled condensation (LVCC) method, which we recently described.[19−23] The LVCC technique uniquely combines the features of pulsed laser vaporization and the controlled condensation process from the vapor phase under well-defined conditions of temperature and pressure in a diffusion cloud chamber. Pulsed laser vaporization offers several important features for the preparation of nanoparticles, such as the production of a high-density vapor of any metal, the generation of a directional high-speed metal vapor for directional deposition of the particles, and the simultaneous or sequential evaporation of several different targets for the preparation of controlled mixtures of nanoparticles as well as nanoparticle alloys.[19−25] It is reasonable to expect that charged nanoparticles (by ions or free electrons) would be formed during the LVCC processes since laser vaporization produces a significant fraction of ions (estimated 10^6 ions and 10^{14} atoms within a 10^{-8} s laser pulse).[19] Recent work indicated that the deposition efficiency of silicon nanoparticles generated by laser ablation was improved by applying an electric field due to the generation of positively charged particles, which were efficiently transferred to the negatively biased electrode.[26] However, no filament assembly was reported.

In the presence of an electric field, the charged particles experience electrophoretic forces, and if the field is nonuniform, the neutral particles experience a translational motion known as dielectrophoresis.[27] Since laser vaporization produces mostly neutral atoms, one expects dielectrophoretic forces to be the major source of nanoparticle assembly. Therefore, it should be possible to influence the growth pattern of nanoparticles by applying an electric field during the condensation process. One can even envisage that charged and neutral nanoparticles may be assembled in the vapor phase, for the first time, under the influence of an electric field. However, the dielectrophoretic effect is proportional to the particle volume and is therefore expected to be much less significant with nanoparticles in the vapor phase (dielectric constant is 1) under realistic electric fields. Thus, our finding that several classes of nanoparticles can be readily assembled in the vapor phase into long filaments and fibers using relatively low DC electric fields is unexpected.

The experimental setup for the LVCC method is shown in Figure 1a. A target of interest (metal, alloy, semiconductor, etc.)

* Corresponding author. E-mail: selshall@hsc.vcu.edu

10.1021/jp022176o CCC: $25.00
Published on Web 03/05/2003

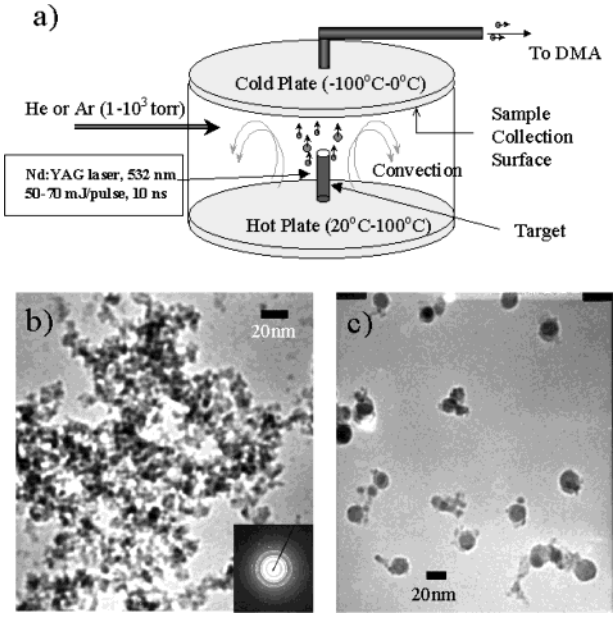

Figure 1. (a) Experimental set up for the preparation of nanoparticles by the LVCC method. (b) TEM image and electron diffraction (ED) pattern of the FeAl intermetallic nanoparticles. The primary particles have average diameters in the range of 8−10 nm. The nanoparticles have the same crystal structure as that of bulk FeAl (B2−CsCl type structure). The lattice parameter for the unit cell of the nanoparticles is calculated as 2.8984, in good agreement with the known lattice parameter of 2.8954 for the bulk material.[22] (c) TEM of 20 nm FeAl nanoparticles selected by a DMA coupled to the LVCC chamber.

is placed on the lower plate of a diffusion cloud chamber, and the chamber is filled with a pure carrier gas such as He (99.99% pure) or a mixture containing a known composition of a reactant gas (e.g., O_2 to form nanoparticle oxides). The metal vapor is generated by pulsed laser vaporization using the second harmonic (532 nm) of a Nd:YAG laser (50−70 mJ/pulse, 10^{-8} s pulse). The DC electric field is applied between the parallel chamber plates, which are separated by a quartz ring of 5 cm height. The top plate is set at a lower temperature than the target and the bottom plate (temperatures are controlled by circulating fluids). The temperature gradient between the bottom and top plates results in a steady convective current, which can be enhanced under high-pressure conditions (10^3 Torr). Convection removes the small particles rapidly from the vaporization region before they grow into larger particles. The nanoparticles are then deposited on the cold top plate. For a precise selection of the particle size, the LVCC method is coupled to a differential mobility analyzer (DMA).[28] The DMA separates the charged nanoparticles based on their electrical mobility. Figure 1b displays a typical TEM image of the nanoparticles prepared by the LVCC method, and Figure 1c demonstrates the DMA size-selection of 20 nm FeAl particles. The X-ray powder diffraction (XRD) of the FeAl nanoparticles exhibits peaks at scattering angles (2θ) of 30.91, 44.15, 64.23, and 81.27 corresponding to scattering from the 100, 110, 200, and 211 planes, respectively of the B2-type crystal lattice.[22]

We investigated the influence of an electric field during the vaporization and condensation of several metallic (Fe, Ti, Ni, Cr, Cu, Zn, Al, In, Pd, Pt), semiconductor (Si, Ge), mixed Si/Pt, intermetallic (FeAl, Ti_3Al, NiAl, and CuZn), and carbon (using a graphite target) nanoparticles. Nanoparticles of intermetallic alloys such as FeAl, NiAl, and Ti_3Al are of special interest because of the important advantages offered by the low density and high strength of the bulk materials.[29] Consolidated intermetallic materials based on nanoparticles may show enhanced plasticity, i.e., they may exhibit significantly better elongations as compared to cast and powder processed components.[29]

Figure 2 displays optical photographs of the LVCC chamber during the preparation of the FeAl and Ti_3Al nanoparticles with an electric field of 60 V/cm applied between the bottom and top plates of the chamber. The nanoparticles assemble as little chains and stack end to end. Generally the chains grow perpendicular on the top and bottom plates of the LVCC chamber as shown in Figure 2a. Eventually, the chains bridge the top and bottom metal plates (electrodes), indicating that both negatively and positively charged particles are involved. Transmission electron microscope (TEM), electron diffraction (ED), and X-ray diffraction (XRD) data of the nanoparticles of the chain filaments are similar to those obtained from the nanoparticles prepared in the absence of the electric field, thus indicating that the field has no effect on the size and composition of the nanoparticles.

With extended laser vaporization times, the filament-like chains grow into 3-D tree-like structures (as in Figure 2b). The chains rotate to orient their dipoles so that the positive end would face the negative end, thus attracting one another. It is interesting to note that these chains stretch at a higher field strength and contract when the field is turned off. This was observed by setting the electric field to zero after the assembly of the filaments between the chamber plates. When a negative voltage of 100 V was applied to the top plate, the filaments inclined toward the negatively charged top plate. On increasing the voltage to −200 V, the filaments inclined more toward the top plate. With further increase in the voltage, the tilting of the filaments continued toward the top plate, thus making an angle of nearly 10−15° with the top plate. By stepwise decreasing of the negative voltage on the top plate, the filaments relaxed back to the original perpendicular orientation [Movie 1 in the Supporting Information]. This observation indicated that the filaments connected to the top negatively charged electrode possess positively charged ends. Thus, the filament chains could be made to rotate by increasing the electric field and in some cases the branches rotated while the trunk remained stationary as shown in Figure 2b.

SEM images of the as-deposited Ti_3Al and FeAl filaments on glass slides placed on the top plate of the LVCC chamber are displayed in Figures 2d and 2e, 2f, respectively. The fiber and the tree-like morphologies of the filaments are quite different from the web-like morphology observed with no electric field applied during the experiment.[19−22] In particular, the photograph and the SEM image of the Ti_3Al filaments, shown in Figures 2c and 2d, respectively, indicate that the filaments condense as a bundle of wires as in a wool yarn. The FeAl filaments tend to exhibit a tree-like morphology with several small branches extending out from a larger trunk as shown in Figure 2e. The filaments can be a few centimeters long and they tangle together with neighboring wires to form bundles.

Filament growth is caused by particle assembly at one of the chamber plates, thereby extending them toward the opposite plate. When the metal target is placed in contact with the bottom plate of the chamber, it creates a gradient in the electric field and causes the filaments to grow toward the target as shown in the photographs of the CuZn nanoparticle fibers displayed in Figure 3(1−6). The filament growth starts as thin small wires extending from the top plate to the center of the CuZn target as shown in Figure 3-1. This pattern continues until the surface of the target is completely covered (Figure 3-3), and then the

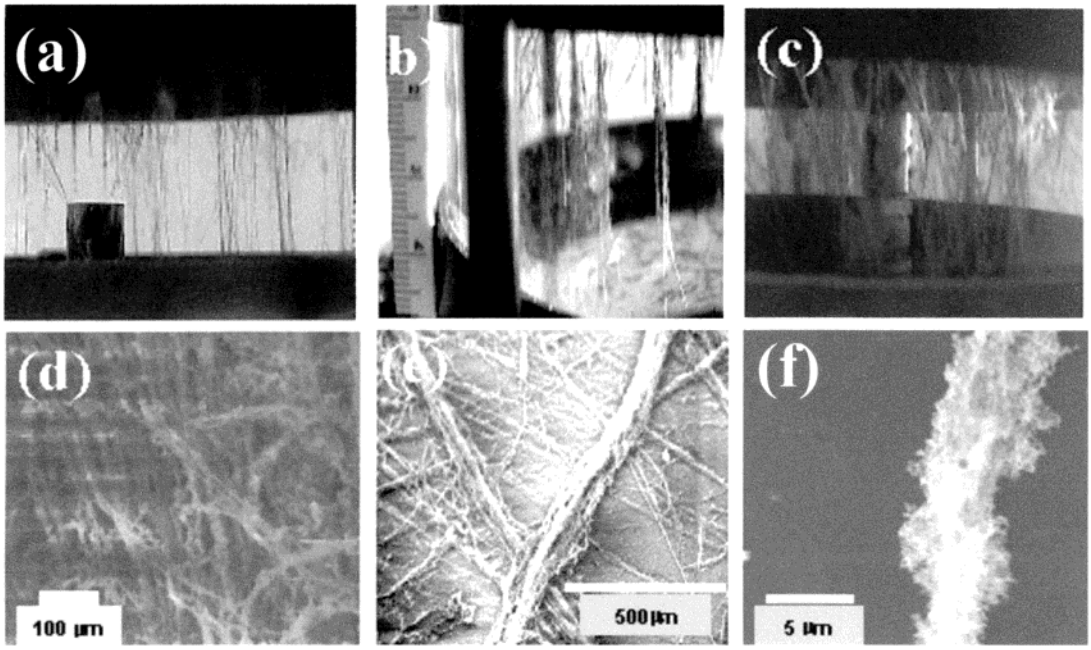

Figure 2. (a) Photograph of FeAl filaments during the early growth time under the influence of 60 V/cm field. (b) Photograph of FeAl tree-like aggregates formed at extended vaporization times in the presence of 60 V/cm field. (c) Photograph of Ti_3Al filaments formed under the influence of 60 V/cm field. (d) SEM of the as-deposited Ti_3Al filaments (scale bar = 100 μm). (e) SEM of the tree-like assembly of FeAl (scale bar = 500 μm). (f) SEM of a single bundle of FeAl nanoparticle aggregate (scale bar = 5 μm).

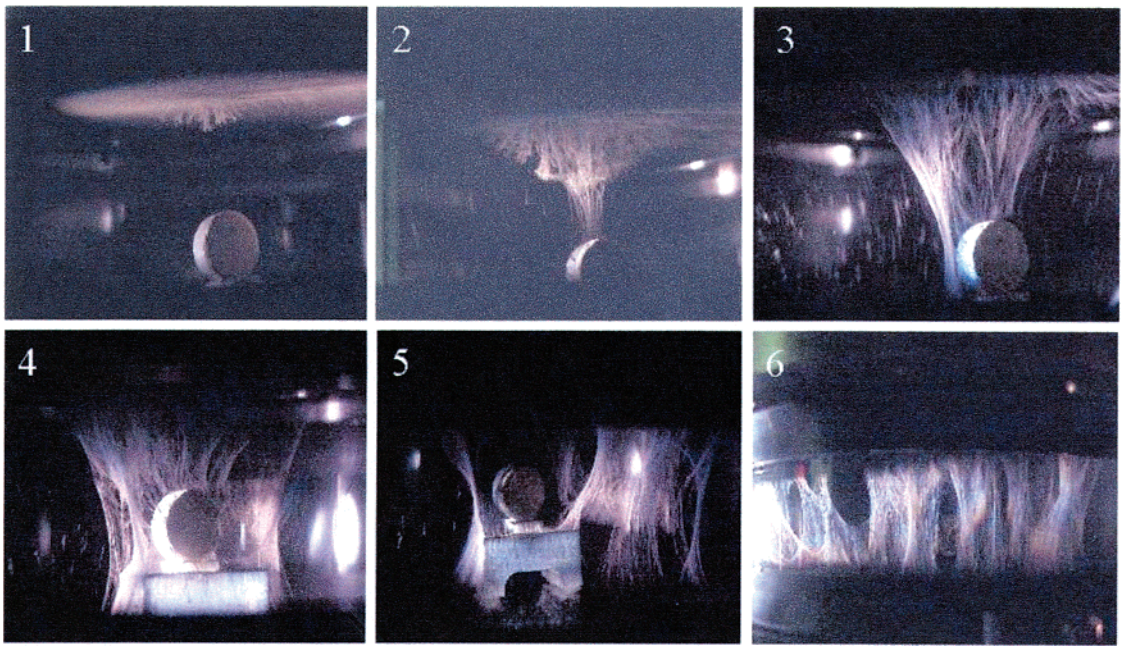

Figure 3. Photographs showing the growth of CuZn nanoparticle fibers at different vaporization times (increasing from 1−6) with 60 V/cm applied field.

filaments start to bridge the top and bottom plates of the chamber. Quite dense fibers can be produced by increasing the amount of nanoparticles formed at extended laser vaporization times as shown in Figure 3-6. The XRD pattern of the nanoparticle filaments is consistent with the γ-Cu_5Zn_8 phase similar to the nanoparticles formed in the absence of an electric field. The TEM analysis indicates that the primary particles are 10−15 nm in diameter.[30]

We carried out several types of experiments to understand the factors controlling the assembly of the nanoparticles. First, we find that the filament growth depends strongly on the type of the nanoparticles assembled. The growth of the carbon filaments is much faster than in the case of metallic or intermetallic nanoparticles. Figure 4a displays an SEM micrograph of the as-deposited carbon filaments obtained from the laser vaporization of a graphite target with an electric field of 20 V/cm applied between the chamber plates. The carbon filaments show a high degree of alignment even after the formation of thick bundles. We note that after extended vaporization times, silicon nanoparticles can be assembled into fractal morphology as shown in Figure 4b. However, the simultaneous laser vaporization of Si−Pt coupled targets resulted in the formation of nearly aligned filaments as shown in Figure 4c. In this experiment, a 2 mm diameter Pt wire was placed

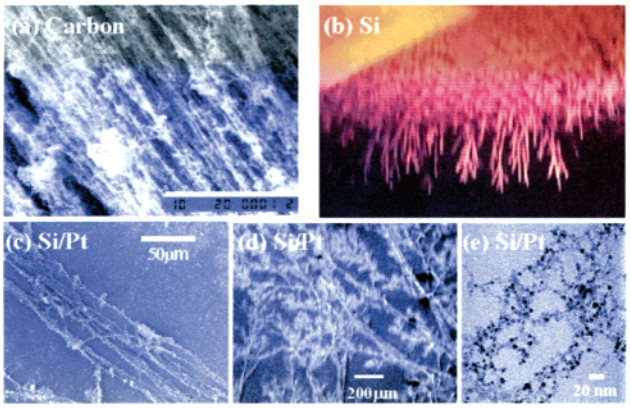

Figure 4. (a) SEM of carbon filaments formed with 20 V/cm applied field (scale bar = 10 μm). (b) Photograph of the fractal growth of Si nanoparticles on the top plate of the LVCC chamber under the influence of 200 V/cm. (c) SEM of nearly aligned Si/Pt nanoparticle filaments formed with 200 V/cm applied field (scale bar = 50 μm). (d) SEM of the dendrite morphology of the Si/Pt nanoparticles formed with 200 V/cm applied field (scale bar = 200 μm). (e) TEM of the Si/Pt nanoparticles resulting from the simultaneous laser vaporization of Pt−Si coupled targets (scale bar = 20 nm).

along the Si target in the center of the laser vaporization spot (the laser was slightly focused into a spherical area of ~8 mm diameter). After extended vaporization times, the Si/Pt nanoparticles assembled into dendritic surface aggregates as shown in Figure 4d. TEM and EDAX of these nanoparticles indicate the formation of shell structures with a Pt core encased within a Si shell, as shown in the TEM image in Figure 4e.

We also find that intermetallic nanoparticles such as FeAl, Ti_3Al, NiAl, and CuZn form filaments more rapidly than do metallic or semiconductor nanoparticles, and they require relatively low electric fields (~20−60 V/cm). Nanoparticles of transition metals such as Ti, Cr, Mn, Fe, Ni, Cu, and Zn can form filaments under the influence of smaller DC fields as compared to the fields required for the assembly of nanoparticles of other main group elements such as Si. No filaments could be observed with Al, Ga, Ge, Sn, Gd, and Er with electric fields up to 200 V/cm. FTIR of the Al, Si, and Ge nanoparticles show peaks associated with different oxide forms. This suggests that surface oxidation affects the charge distributions on the surfaces of the nanoparticles in a way that weakens the electrostatic interactions among the nanoparticles and therefore inhibits the formation of the filaments. Also, no filaments were observed for oxide intermetallic nanoparticles produced in the presence of a relatively low concentration of O_2 (7% of the total pressure in the chamber). In general, we find that field strength and particle number density deposited on the top plate are the most important factors in filament growth because they must exceed threshold values in order for the filaments to start growing. Table 1 lists the types of nanoparticles investigated for the formation of filaments in the presence of DC electric fields.

To explore whether the electric field can be used to form more complex structures, we grew Ni filaments in the presence of an olefin monomer (isobutene). The gas-phase polymerization of isobutene assisted by plasma laser vaporization and the catalytic effect of the Ni nanoparticles resulted in the formation of tree-like aggregates involving multiple branching of carbonaceous polymer/metal composites, as shown in Figure 5a. In the absence of the electric field, the polymer/Ni nanoparticle composite did not exhibit the tree-like morphology, as shown in Figure 5b. The composite appears to be a cross-linked carbonaceous polymer with an amorphous XRD pattern and no appreciable solubility in organic solvents.

TABLE 1: Electric Field (DC) Effects on the Formation of Nanoparticle Filaments

nanoparticles forming filaments	electric field used (V/cm)	nanoparticles with no filaments' formation	electric field used (V/cm)
In	200	Ga	200
Si	200	Al	500
Mg	100	B	200
Fe	40−60	Ge	200
Cu	40−60	Sn	200
Zn	40−60	Gd	100
Ti	40−60	Er	100
Ni	40−60		
carbon	10−20		
FeAl	10		
Ti_3Al	20		
NiAl	20		

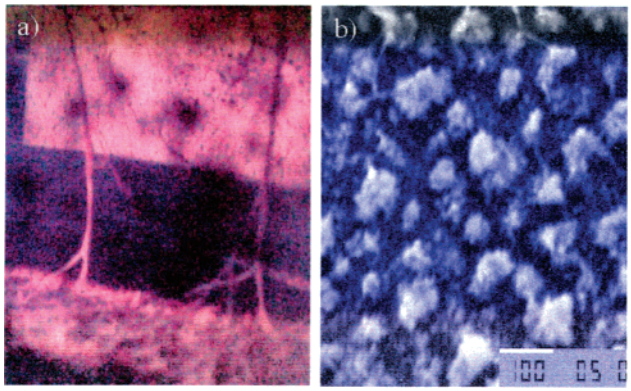

Figure 5. (a) Photograph of the filament and tree-like aggregates of Ni−polymer composites grown in the presence of 60 V/cm field across the LVCC chamber. (b) SEM of polyisobutene beads containing Ni nanoparticles produced in absence of electric field (scale bar = 100 μm).

The effect of the electric field on the formation of the chain aggregates acts through the polarization of the charges on the nanoparticle surface.[27] For larger particles, the effect of the electrostatic charge is overpowered by the effect of gravity, but for nanoparticles the electrostatic forces will be predominant. We believe that there is a mixture of positive and negative charges on the surfaces of the nanoparticles and that some of the nanoparticles will have net charges. The nanoparticles with net charges will respond to the electric field with the electrophoretic force. However, the neutral particles will experience a dielectrophoretic force caused by polarization effects.[27] Our results can be explained within the framework of combined electrophoresis and dielectrophoresis effects.[27] It appears that the initial nucleation and growth starts with the ions (electrophoretic effect) followed by accretion of neutral atoms and clusters (dielectrophoretic effect). Specifically, there are two effects that when combined may lead to the sticking of particles of the same net charge. The dipole force is very strong near the surface of the particle; further away from the surface, the net charge or monopole force becomes more effective. When two individual particles are separated by a certain distance, they will respond to the monopole charge between them, and if the monopoles are the same, the particles will repel. However, by orienting their dipoles so that they are attracting one another, and since at this short distance the dipole dominates over the net charge, the two particles will stick together. The observations of enhanced assemblies of intermetallic and transition metal nanoparticles are consistent with the significant dipole forces and electronic polarizability, respectively, in these systems.

The results of this work have important implications, not only on the growth and assembly of nanoparticles from a materials

point of view but also for the role of nanoparticles in environmental, atmospheric, astrophysical, and astrochemical processes. Understanding the mechanisms of nanoparticle chaining can lead to full control of the growth of nanoparticles into filaments and tree-like assemblies. These materials could be used for the generation of designed aerosols and "smart dust", which could have important applications in the detection and monitoring of trace components in the vapor phase.

Another important implication of the present work is related to the role of nanoparticles in the formation of interstellar dust and in initiating heterogeneous nucleation and catalytic reactions. For example, nano- and submicron metal, metal oxide, and silicate particles are known to form in the solar nebula and may be responsible for its opacity.[31] The metal and oxide nanoparticles provide catalytic surfaces upon which gaseous molecules may condense, and when irradiated by photons and cosmic rays they become efficient nanofactories for astrochemical organic synthesis.[32] As shown here, the metal nanoparticles may catalyze reactions leading to the formation of carbonaceous polymer−metal composites. It is interesting that the polymer−rock composites are observed directly in collected "tar ball" particles and in cometary rocky/carbon composite grains.[31,33]

In conclusion, electric field-assisted assemblies of semiconductor, metallic, and intermetallic nanoparticles from the vapor phase have been demonstrated. The alignment forces result from the polarization of the nanoparticles in the electric field. The LVCC method provides a general and rational approach for the assembly of nanoparticles from the vapor phase into fibers and networks that can bridge the nanometer through centimeter size regimes. These assemblies not only represent the building blocks for functional devices for future nanotechnologies, but also provide good models to simulate the effects of electric and magnetic fields, the adsorption and the catalytic reactions of organic vapors on the grain surfaces in space.

Acknowledgment. The authors gratefully acknowledge support from the NSF (Grant CHE 98 16536), the NASA Microgravity Materials Science Program (Grant NAG8-1484) and Chrysalis Technologies Incorporated.

Supporting Information Available: Digital movie showing the motion of the nanoparticle filaments induced by the electric field. This material is available free of charge via the Internet at http://pubs.acs.org.

References and Notes

(1) Edelstein, A. S.; Cammarata, R. C. *Nanomaterials: Synthesis, Properties and Applications*; Institute of Physics: Bristol and Philadelphia, 1996.

(2) Chow, G. M.; Gonsalves, K. E. *Nanotechnology: Molecularly Designed Materials*; ACS Symposium Series 622; American Chemical Society: Washington, DC, 1996.

(3) Alvisatos, A. P. *J. Phys. Chem.* **1996**, *100*, 13226.

(4) Hu, J.; Odom, T. W.; Lieber, C. M. *Acc. Chem. Res.* **1999**, *32*, 435.

(5) Huang, Y.; Duan, X.; Wei Q.; Lieber, C. M. *Science* **2001**, *291*, 630−633.

(6) Cui, Y.; Wei, Q.; Park, H.; Lieber, C. M. *Science* **2001**, *293*, 1289−1292.

(7) Martin, C. R. *Science* **1994**, *266*, 1961−1966.

(8) Sapp, S. A.; Mitchell, S. T.; Martin, C. R. *Chem. Mater.* **1999**, *11*, 1183.

(9) Sun, L.; Searson, P. C.; Chien, C. L. *Science* **1999**, *74*, 2803.

(10) Hermanson, K. D.; Lumsdon, S. O.; Williams, J. P.; Kaler, E. W.; Velev, O. D. *Science* **2001**, *294*, 1082−1086.

(11) Smith, S. A.; Nordquist, T. J.; Mayer, T. S.; Martin, B. R.; Mbindyo, J.; Mallouk, T. E. *Appl. Phys. Lett.* **2000**, *77*, 1399−1401.

(12) Liu, J.; Lee, T.; Janes, D. B.; Walsh, B. L.; Melloch, M. R.; Woodall, J. M.; Reifenberger, R.; Andres, R. P. *Appl. Phys. Lett.* **2000**, *77*, 373−375.

(13) Vigolo, B.; Penicaud, A.; Coulon, C.; Sauder, C.; Pailler, R.; Journet, C.; Bernier, P.; Poulin, P. *Science* **2000**, *290*, 1331−1334.

(14) Bower, C.; Zhou, W.; Jin, S.; Zhou, O. *Appl. Phys. Lett.* **2000**, *77*, 830.

(15) Avigal, Y.; Kalish, R. *Appl. Phys. Lett.* **2001**, *78*, 2291.

(16) Zhang, Y.; Chang, A.; Cao, J.; Wang, Q.; Kim, W.; Li, Y.; Morris, N.; Yenilmez, E.; Kong, J.; Dai, H. *Appl. Phys. Lett.* **2001**, *79*, 3155.

(17) Wu, Y.; Yang, B. *Nano Lett.* **2002**, *2*, 355−359.

(18) Lee, G, H.; Huh, S. H.; Park, J. W.; Jeong, J. W. *J. Phys. Chem. B* **2002**, *106*, 2123−2126.

(19) El-Shall, M. S.; Li, S. Synthesis and characterization of metal and semiconductor nanoparticles. In *Advances in Metal and Semiconductor Clusters*; Duncan, M. A., Ed.; JAI Press Inc.: London, 1998; Volume 4, Chapter 3, pp 115−177.

(20) Li, S.; Silvers, S.; El-Shall, M. S. *J. Phys. Chem. B* **1997**, *101*, 1794.

(21) Germanenko, I. N.; Li, S.; El-Shall, M. S. *J. Phys. Chem. B* **2001**, *105*, 59−66.

(22) Pithawalla, Y. B.; El-Shall, M. S.; Deevi, S. C.; Rao, K. V. *J. Phys. Chem. B* **2001**, *105*, 2085−2090.

(23) See also: U.S. patent 5,580,655, *Silica Nanoparticles*; M. S. El-Shall, D. Graiver, U. C. Pernisz, December 3, 1996; U.S. patent 5,695,617, *Silicon Nanoparticles*, D. Graiver, U. C. Pernisz, M. S. El-Shall, December 9, 1997; U.S. patent 6,136,156, *Nanoparticles of Silicon Oxide Alloys*, M. S. El-Shall, D. Graiver, U. C. Pernisz, October 24, 2000; U.S. patent 6,368,406, *Nanocrystalline Intermetallic Powders Made by Laser Evaporation*, S. C. Deevi, Y. B. Pithawalla, M. S. El-Shall, April 9, 2002.

(24) Gnedovets, A. G.; Gusarov, A. V.; Smurov, I. *J. Phys. D: Appl. Phys.* **1999**, *32*, 2162.

(25) Geohegan, D. B.; Puretzky, A. A.; Duscher, G.; Pennycook, S. J. *Appl. Phys. Lett.* **1998**, *72*, 2987.

(26) Muramoto, J.; Sakamoto, I.; Nakata, Y.; Okada, T.; Maeda, M. *Appl. Phys. Lett.* **1999**, *75*, 751−753.

(27) Pohl, H., A. *Dielectrophoresis*; Cambridge University Press: London, 1978.

(28) Seto, T.; Kawakami, Y.; Suzuki, N.; Hirasawa, M.; Aya, N. *Nano Lett.* **2001**, *1*, 315−318.

(29) Deevi S. C., Liu, C. T., Yamaguchi, M., Eds. *Intermetallics for the Third Millennium, Intermetallics* 2000, 8.

(30) Pithawalla, Y. B.; El-Shall, M. S.; Deevi, S. *Scr. Mater.* **2003**, *48*, 671.

(31) Cernicharo, J.; Heas, A. M.; Tielen, A. G. G. M.; Pardo, J. R.; Herpin. F.; Guelin, M.; Waters, L. B. F. M. *Astrophys. J.* **2001**, *546*, L123−L126.

(32) Henning, Th. *Chem. Soc. Rev.* **1998**, *27*, 315.

(33) Bernstein, M. P.; Sandford, S. A.; Allamandola, L. J. *Sci. Am.* **1999**, July 27.